Effect of high current density on the admittance response of interface states in ultrathin MIS tunnel junctions.

Christian Godet, Alain-Bruno Fadjie-Djomkam, Soraya Ababou-Girard

Solid State Electronics

Effect of high current density on the admittance response of interface states in ultrathin MIS tunnel junctions

Christian Godet,[a] Alain-Bruno Fadjie-Djomkam, Soraya Ababou-Girard,

Institut de Physique de Rennes, CNRS UMR 6251, Université de Rennes 1, Campus de Beaulieu, 35042 Rennes Cedex, France

a) Author to whom correspondence should be addressed ;

electronic mail: *christian.godet@univ-rennes1.fr*

****

Corresponding author :

Christian GODET
EPSI – IPR (Bât. 11C - Beaulieu)
Université Rennes 1
35042 RENNES (France)

Tél : +33 2 23 23 57 06
Fax : +33 2 23 23 61 98
Mél : christian.godet@univ-rennes1.fr

Abstract

The effect of a high current density on the measured admittance of ultrathin Metal – Insulator – Semiconductor (MIS) tunnel junctions is investigated to obtain a reliable energy distribution of the density, $D_S(E)$, of defects localized at the semiconductor interface. The behavior of admittance $Y(V, T, \omega)$ and current density $J(V, T)$ characteristics is illustrated by rectifying Hg // $C_{12}H_{25}$ – Si junctions incorporating *n*-alkyl molecular layers (1.45 nm thick) covalently bonded to *n*-type Si(111). Modeling the forward bias admittance of a non equilibrium tunnel junction reveals several regimes which can be observed either in $C(\omega \approx 0)$ vs (J) plots of the low frequency capacitance over six decades in current or in $M''(\omega)$ plots of the electrical modulus over eight decades in frequency. At low current density, the response of interface states above mid-gap is unaffected and a good agreement is found between the interface states densities derived from the modeling of device response time $\tau_R(V)$ and from the low–high frequency capacitance method valid for thick MIS devices; the low defect density near mid-gap ($D_S < 10^{11}$ $eV^{-1}.cm^{-2}$) results from a good passivation of dangling bonds at the $C_{12}H_{25}$ – *n* Si interface. In the high current density regime ($J > 1$ $mA.cm^{-2}$), the admittance depends strongly on both the density of localized states and the dc current density, so that the excess capacitance method overestimates D_S. For very high current densities ($J > 10$ $mA.cm^{-2}$), the observation of a linear $C(\omega \approx 0)$ vs (J) dependence could indicate some Fermi level pinning in a high interface density of states located near the Si conduction band. The temperature-independent excess capacitance $C(\omega \approx 0)$ - C(1 MHz) observed at very small J, not predicted by the admittance model, is attributed to some dipolar relaxation in the molecular junction.

1. Introduction

The development of Metal-Insulator-Semiconductor (MIS) junctions with ultra-thin insulator (d_T < 3 nm) has stimulated the study of new insulating materials, such as saturated organic chains with a wide electronic band gap (≈ 7 eV).[1] In the field of hybrid molecular-silicon junctions, alkyl-based devices have been investigated for fundamental studies of transport mechanisms (thermionic emission, tunnelling, recombination) while applications are foreseen in the fields of solar cells and gate insulators.[2,3] Alkyl monolayers may form a well controlled interlayer for further assembly of nanoscale objects (molecules, nanoparticles, nanotubes) providing new functionalities to form original devices and circuit architectures.[4-8]

Covalent binding of linear saturated (*n*-alkyl) chains to hydrogenated Si(111):H surfaces[9] forms robust molecular layers with a high coverage which play the role of a nanometer-thick tunnel barrier. Due to sterical constraints, the density of surface Si-H sites which are not grafted with alkyl molecules is larger than 4×10^{14} cm^{-2} (≈60% of surface Si atom density); however, the density of electrically active defects, D_S, remains relatively small, at least immediately after grafting, in the 1×10^{10} - 3×10^{11} $eV^{-1}.cm^{-2}$ range.[10-15] However, besides the problem of engineering a homogeneous and reliable top electrode in contact with a nanometer-thick molecular monolayer, a major issue in hybrid molecular-silicon junctions is the structural disorder which results from the irreversible grafting mechanism related to the strong covalent bonding ; hence structural disorder probably induces some distribution of barrier heights for electrical transport and may explain the wide range of conductance values observed experimentally.[16,17]

In metal / semiconductor (SC) junctions, the presence of interface states and of a thin insulating layer have been recognized as non idealizing factors in the current-voltage (*I*-*V*) characteristics.[18-21] A number of methods based on *non-stationary* measurements have been developed for interface defect characterization in thick MIS diodes[22,23] and tentatively extended to MIS junctions with interfacial layers,[24,25] ultrathin SiO_2,[19,26-29] and molecular insulator.[3,14,15,30]

In the latter devices, frequency and temperature dependence of molecular MIS admittance brings valuable information to discriminate interface states response and dipolar relaxation effects.[14,31-33]

MIS tunnel diodes are *non equilibrium* devices due to the large current density flowing through the thin insulating layer **(Figure 1).** It has been shown that, between 1 and 2 nm thick SiO_2, the quasistatic hypothesis progressively fails and a kinetic approach should be developed;[34] this effect is expected to occur at larger thickness values for an insulator with a lower tunnel barrier height. We must then calculate the position of the quasi-Fermi level at the interface, its value depending on the applied voltage, on the transmission coefficient of the barrier (i.e. essentially on the insulator thickness) and on the interface defects. The *non-stationary* transport properties (capacitance and conductance) of ultrathin MIS tunnel junctions and non-abrupt MS junctions under modulated bias, $V + V_{AC} \exp(j\omega t)$, have been derived by Gomila[35,36] using coupled kinetic equations which define the occupancy of interface states as a function of applied dc bias, V, bias modulation frequency, ω, and temperature, T. In contrast with previous models, exchange of carriers between interface states and either the metal or the semiconductor has been considered. However, to our best knowledge, no systematic validation of Gomila's model has been performed with experimental data for tunnel MIS diodes.

In this work, the behavior of admittance $Y(V, T, \omega)$ and dc current density $J(V, T)$ characteristics in ultrathin MIS tunnel junctions is illustrated by Hg // $C_{12}H_{25}$ – *n* Si junctions incorporating *n*-alkyl molecular layers (d_T = 1.45 nm) covalently bonded to *n*-type Si(111). In order to obtain a reliable density of states distribution from admittance measurements in non equilibrium MIS devices, this work emphasizes the combined role of dc current density and interface states density, as predicted by the tunnel barrier model. The strong rectification in $J(V, T)$ due to the *n*-type doping provides a very large range of dc current which is helpful to identify several transport regimes.

The organization of the manuscript is as follows. **Section 2** recalls the physics of the tunnel barrier model leading to the admittance $Y(V, T, \omega)$ of ultrathin MIS tunnel junctions. The combined role of dc current density $J(V, T)$ and interface states density distribution $D_S(E)$ in the measured admittance characteristics, in particular the *low frequency capacitance* and *high frequency conductance*, is emphasized and the device response time is introduced. **Section 3** describes the experimental methods, including photochemical grafting of alkene molecules on Si(111), X-ray photoelectron spectroscopy (XPS) characterization of molecular coverage, spectroscopic ellipsometry (SE), dc and ac electrical transport at variable T. Besides $J(V, T)$ measurements in the T range 243-293 K, the admittance $Y(V, T, \omega)$ is characterized in a wide frequency range (10^{-2} to 10^{7} Hz) in order to investigate the dynamic characteristics of the tunnel barrier, the space charge region and the interface trap distribution. **Section 4** is devoted to the admittance spectroscopy characteristics, used to obtain the flat band voltage, V_{FB}, the device response time, τ_R, and the density of interface electronic states, $D_S(E)$. The comparison of the density of states distributions derived from the device response time and from the classical low – high frequency capacitance method (valid for thick MIS devices), respectively, allows to define a "low current density regime" and a "high current density regime". The potential influence of high local current density, e.g. due to some lateral inhomogeneity of the barrier height, on the measured admittance $Y(V, T, \omega)$ is also discussed.

Our experimental results are compared with some predictions of admittance modeling for ultrathin MIS tunnel junctions, in particular the dependence of the low frequency capacitance $C(\omega \approx 0)$ on $J(V, T)$ and the frequency dependence of the electrical modulus. Some model parameters such as the microscopic response time of interface defects and their distribution in energy, $D_S(E)$, are derived from experimental data. While all of the experimental results presented in this work were obtained using Hg // $C_{12}H_{25}$ – *n* Si (111) molecular junctions, the method is more general and could be applied to any tunnel MIS device.

2. Non stationary transport model

The non-stationary transport properties (capacitance and conductance) of non intimate Schottky contacts and MIS tunnel diodes have been derived using coupled kinetic equations which define the occupancy of interface states as a function of applied dc bias, bias modulation frequency and temperature.[35,36] We briefly recall the main hypothesis and the device admittance expression to emphasize the combined role of dc current density $J(V, T)$ and interface states density distribution $D_S(E_C - E_T)$ in the *low frequency capacitance* and *high frequency conductance* and to introduce the device response time directly evidenced in $M''(\omega)$ plots of the electrical modulus.

2.1 Kinetic mechanisms

In the energy band diagram of the MIS tunnel diode with insulator thickness d_T (noted as δ in **Figure 1**), the barrier height, ϕ_{BN}, is defined by the metal work function, ϕ_m, and the SC electron affinity, χ. The dc thermionic emission current across the interface is governed by this barrier height and by an attenuation factor exp(- $\beta^{o} d_T$) due to the tunnel barrier transparency; the parameter β^{o} can be derived from the temperature dependence of the apparent barrier height in the thermionic emission regime.[15]

Figure 1 shows that three elementary kinetic processes can be identified:

$$q_n \leftrightarrow q_m ; \quad q_s \leftrightarrow q_m ; \; q_s \leftrightarrow q_n \qquad (1)$$

in which q_n, q_m, q_s stand respectively for the electrons in the semiconductor, in the metal and at the interface states. If the series resistance (R_S) can be neglected (not true at high J), the applied bias V is the difference $F_m - F_n$ between the metal Fermi level, F_m, and the semiconductor Fermi level, F_n.

In contrast with Gomila's approach, where no restriction on the carrier exchange between interface states and either the metal or the semiconductor has been assumed, previous models of thin MIS junctions restricted the exchange of electrical carriers of interface traps to the SC conduction band.[25,29,37,38] Although resulting expressions of the admittance are quite similar to **Equation 12**, the microscopic response times of localized interface states are quite different: a capture-emission time constant is derived from Shockley-Read-Hall parameters[22] in the former models,[37-40] in contrast with the tunnel response time **(Eqn 7)** in Gomila's model.[36]

2.2 Device admittance

The influence of the dc current density on the device admittance is qualitatively described by the "trap transistor model": the out-of-phase modulation of interface charge (Q_{SS}) is responsible for an out-of-phase modulation of the electric field in the insulator and of the SC band bending $\delta\Psi_S$, which in turn produces an ac-current $\delta J = J\ (q\ \delta\psi_S/kT)$ and results in a large capacitance at low frequency $C(\omega \approx 0)$.[25]

The voltage drop Δ on the insulator (**Figure 1**) is related to the accumulated charge per unit area at the SC surface and in the space-charge layer (Gauss's law):

$$\Delta = (\phi_m - \chi) - \phi_{BN} = -\frac{q}{C_i}\{n_{SS}(F_S - E_V) - N_{DS}\} + \frac{Q_{SC}}{C_i} \qquad (2)$$

where the number $n_{SS}(F_S - E_V)$ of occupied interface states per unit area is a function of the surface Fermi level position (F_S) with respect to the valence band energy (E_V), N_{DS} is the density of donor states at the interface. The charge in the semiconductor, $Q_{SC} = (2q\varepsilon_S N_D\psi_S)^{1/2}$, is given by the permittivity ε_S, the dopant density N_D, and the band bending ψ_S. $C_{SC} = \varepsilon_S / w$ and C_i are respectively the SC and the insulator capacitance values per unit area.

All relevant transport parameters can be determined from the position of the surface Fermi level, F_s, and the transition coefficients (λ_{nm}, λ_{sm}, λ_{sn}) corresponding to the elementary

processes represented in **Equation 1.** Note that coefficients λ_{nm} and λ_{sm} (cm^{-2} s^{-1}) both incorporate a tunnel barrier attenuation coefficient, exp(- $\beta^{\circ}d_T$). The total current density J flowing through the system is given by $J = \frac{\partial D}{\partial t} + J_n$, where $D = \varepsilon E$ and $J_n = J_n^{TE} + \frac{J_S}{1+\alpha}$ is the sum of thermionic emission and interface states current densities:

$$J_n^{TE} = -qN_C V_R \ \exp(-q\beta\phi_{bn}) \ \left[1 - \exp\left(\beta(F_n - F_m)\right)\right] \qquad (3)$$

$$J_s = -q\lambda_{ns}(1+\alpha)\exp(-q\beta\phi_{bn})\left(\exp\left(\beta(F_s - F_m)\right) - \frac{1+\alpha^{-1}\exp\left(\beta(F_n - F_m)\right)}{1+\alpha^{-1}}\right) \qquad (4)$$

$$\alpha = \frac{\lambda_{sm}}{\lambda_{sn}} = \exp\left(\frac{qV_C}{kT}\right) \text{ and } N_C V_R = \lambda_{nm} + \frac{\exp(E_G/kT)}{\lambda_{sn}^{-1} + \lambda_{sm}^{-1}} \qquad (5)$$

Here $\beta = 1/kT$ and V_C is a critical bias (assumed to be a constant) which characterizes the interface states occupation under non equilibrium.[35] Using the ac expression of the charge conservation equation $J_S + q\frac{\partial n_{SS}}{\partial t} = 0$, at the interface states, one obtains the out-of-phase modulation of the surface Fermi level position

$$\frac{\delta(F_S - F_m)}{\delta V} = q\left[\frac{\exp q\beta(V - V_C)}{(1+j\omega\tau)(1+\exp q\beta(V - V_C))}\right] \qquad (6)$$

where

$$\tau = \frac{D_{s\alpha}}{\beta\lambda_{ns}\alpha\exp\left(-q\beta\phi_{BN}^{dc}\right)} \qquad (7)$$

is the microscopic tunnel response time and

$$D_{s\alpha} = D_S\left(1 - \frac{1}{q}\frac{\partial(F_s - F_m)}{\partial V}\right), \quad D_{sb} = D_S\left(\frac{1}{q}\frac{\partial(F_s - F_m)}{\partial V}\right), \quad D_S = \left.\frac{\partial n_{SS}}{\partial E_{F_S}}\right|_{E_{FS} - E_V^0} \qquad (8)$$

are the fractions of the total density of states $D_S(E)$ in equilibrium with the metal or the SC, respectively. In ac mode, a small-signal analysis provides the total ac current

$$\delta J = j\omega\delta Q_{SC} + \delta J_n^{TE} + \frac{\delta J_S}{1+\alpha} \qquad (9)$$

The expressions of the ac current and admittance simplify for forward bias values, $V > V_C$, where the fraction of interface states in equilibrium with the metal can be neglected ($D_{sa} \approx 0$) hence $D_S \approx D_{sb}$, the density of states in equilibrium with the semiconductor.[36] The junction admittance, $Y(\omega) = \delta J/\delta V$, is given by:

$$Y(\omega) = G + j\omega C = q\beta J_0 + \left[q\beta J_{dc} + \frac{G_S}{1+\alpha} + j\omega\left(C_{sc} + \frac{C_S}{1+\alpha}\right)\right] \times \frac{j\omega C_i}{G_S + j\omega(C_i + C_{SC} + C_S)} \qquad (10)$$

In **Eqn. 10,** the square bracket is $(\delta J/\delta\psi_S)$, the last fraction is $(\delta\psi_S/\delta V)$ and the interface states capacitance and conductance per unit area, defined by the relation $q\delta J_S = (G_S + j\omega C_S)\delta\psi$, have been introduced:

$$G_S = \omega^2\tau \frac{q^2 D_S}{1+\omega^2\tau^2} \qquad (11a) \qquad C_S = \frac{q^2 D_S}{1+\omega^2\tau^2} \qquad (11b)$$

Using $C_\Sigma = C_i + C_{SC}$, the MIS conductance and capacitance per unit area are:

$$\hat{G} = q\beta J_0 + \frac{q\beta J C_i(C_S + C_\Sigma) + C_i^2 G_S\left(\frac{1-\alpha C_{SC}/C_i}{1+\alpha}\right)}{\left(\frac{G_S}{\omega}\right)^2 + (C_S + C_\Sigma)^2} \qquad (12a)$$

$$\hat{C} = C_i \frac{q\beta J \frac{G_S}{\omega^2} + \frac{(G_S/\omega)^2}{1+\alpha} + (C_S + C_\Sigma)\left(\frac{C_S}{1+\alpha} + C_{SC}\right)}{\left(\frac{G_S}{\omega}\right)^2 + (C_S + C_\Sigma)^2} \qquad (12b)$$

We further derive approximations of the low frequency capacitance $C(0)$ and high frequency conductance $G(\infty)$

$$\hat{G}(\infty) = q\beta J_0 + \frac{q\beta J C_i C_\Sigma + q^2 D_S \tau^{-1}\left(\frac{1-\alpha C_{SC}/C_i}{1+\alpha}\right) C_i^2}{C_\Sigma^2} \qquad (13)$$

$$\hat{C}(0) = C_i \frac{q\beta J q^2 D_S \tau + \left(\frac{q^2 D_S}{1+\alpha} + C_{SC}\right) C_\Sigma}{{C_\Sigma}^2} \qquad (14)$$

which are particularly interesting to assess the role of the current density through the tunnel MIS diode in the measured admittance. Considering the role of D_S, τ and J in admittance spectroscopy data, the $D_S\tau$ product and J_{dc} are strongly coupled in the excess capacitance

$$C(0) - C(\infty) \approx q^2 D_S \left(1 + \frac{q\beta J \tau}{C_i}\right) \qquad (15)$$

while only $D_S\tau^{-1}$ appears in the excess conductance due to interface states (for $q^2 D_S \ll C_i$)

$$G(\infty) - G(0) \approx q^2 D_S \tau^{-1} (C_i/C_\Sigma)^2 \approx q^2 D_S \tau^{-1} \qquad (16).$$

In principle, the magnitude of τ and $D_S\tau$ values can be derived from $C(0)$ vs J plots in some particular conditions, since **Eqn 15** predicts an inflexion point at $J \approx C_i / q\beta\tau$, whereas a linear regime is expected at very high current densities, if D_S is a constant, with a slope $(q^3 D_S \beta\tau / C_i)$.

Simulations of the admittance (**Fig. 2-3**) were performed using experimental current density $J(V)$ data (**Figure 4**), device area $S = 5\times10^{-3}$ cm^2 and variable D_S values in the range 10^8 - 10^{13} eV^{-1}.cm^{-2}. The respective effects of the current density (forward bias) and defect density on the conductance, capacitance and electrical modulus are shown in **Figure 2**.

For comparison with experimental results (**Fig. 5-8**), we have chosen to include in the model the effect of a series resistance (R_S = 100 Ω) on the admittance.[38] Note that high values of the series resistance R_S limit the frequency range where interesting physical mechanisms can be observed, typically below 1 MHz in this study. Complementary experiments have shown that the R_S value can be decreased by using a higher Si doping level. As discussed in **Section 4.2**, R_S can be obtained experimentally in the high frequency regime where $G(\omega)$ is proportional to ω^2.

2.3 Device response time

For a parallel *R-C* circuit, the calculated device response time, $\tau_R(V,T) = (C/G)$, is a physical quantity which can be readily compared with experimental values of the inverse angular frequency, $\tau_R = \omega_{MAX}^{-1}$, at the maximum of the imaginary part of either the impedance $Z''(\omega)$ or electrical modulus $M''(\omega)$ plots. The effects of a high current density can be qualitatively derived for a junction with a low defect density ($C_S << C_{SC}$); in the low frequency limit ($\omega\tau \ll 1$) the tunnel barrier model (**Eqn 12**) gives a junction response time $\tau_R(V,T)$ which depends on the density of localized states D_S and on the dc current density J through the junction:

$$\tau_R \approx \frac{q\beta J q^2 D_S \tau + C_{SC} C_i}{(q\beta J) C_i} \qquad (17)$$

where τ is defined by **Eqn 7.** Hence, the response time is larger than in the ideal case ($\tau_R \approx \frac{C_{SC}}{q\beta J}$) obtained with no defects (D_S = 0).

In this Section, we focus on the behavior of $M''(\omega) = C_0\,\omega\,[G(1 + R_S G) + R_S\omega^2 C^2]/(G^2 + \omega^2 C^2)$, where we have included the effect of a series resistance (R_S) on the measured admittance and C_0 is an arbitrary normalization factor (100 pF). Using the same parameters as in **Figure 2c** and a current density $J = 1\times10^{-7}$ A.cm^{-2} (corresponding to + 0.1 V bias and 293 K), **Figure 3a** shows that $M''(\omega)$ plots present two maxima corresponding respectively to the semiconductor (LF) and to the tunnel barrier (HF). For very low D_S values, the low frequency response occurs at $f^{LF} = (G/2\pi C_{SC})$ while the high frequency response at $f^{HF} = 1/2\pi\tau$ is related to the microscopic tunnel response time.

The electrical modulus $M''(\omega)$ has been simulated over a wide range of D_S values (10^8 - 10^{13} eV^{-1}.cm^{-2}). **Figure 3b** shows that the two peaks shift in opposite directions with increasing density of localized states, namely f^{LF} decreases because $C(0)$ increases while f^{HF} increases because $G(\infty)$ increases. We have also reported the peak intensities which also change in

opposite directions; basically, with increasing D_S, M_{MAX}^{LF} decreases because $C(0)$ increases while M_{MAX}^{HF} increases because $G(\infty)$ increases. **Figure 3b** corresponds to a low current density (1×10^{-7} A.cm^{-2}); however, with increasing forward bias, f^{LF} will increase exponentially and may eventually approach f^{HF}, as illustrated by experimental data in **Figure 8a**.

Since the low frequency response dominates $M''(\omega)$ plots in device-quality MIS tunnel junctions (typically $D_S < 1\times10^{11}$ eV^{-1}.cm^{-2}), the experimental evolution of both f^{LF} and M_{MAX}^{LF} values may give valuable information on the distribution $D_S(E)$. These methods are essentially sensitive in the range 2×10^{9} - 2×10^{11} eV^{-1}.cm^{-2} where M_{MAX}^{LF} decreases over one decade (**Fig. 3b**). In a previous report,[15] the response time $\tau_R(V,T,D_S)$ of the tunnel MIS device has been used to derive $D_S(E_C - E_T)$. In this work, a more complete analysis is proposed to check the consistency of both methods.

2.4 Barrier height distribution

An important assumption of the model is that the density of interface states and the current density through the device are laterally homogeneous. In the case of inhomogeneous interface potential providing low barrier height patches, it has been shown that a small fraction of the device area may be responsible for a significant fraction of the dc current through Schottky barrier devices, in particular at low bias and low temperature.[39-41] A similar effect has been observed in molecular tunnel junctions, after ageing at the ambient.[42]

In this case, for a given applied bias value, low barrier height patches with a high local dc current density may result in a distribution of τ values (tailing towards shorter times, **Eqn 7**). As a consequence, the interface states conductance $G(\omega)$ is a sum (weighted by the effective patch area S_i) of local conductance values $G_i(\omega)$ defined by their characteristic angular frequency τ_i^{-1} and high frequency plateau $q^2 D_S \tau_i^{-1}$ value (**Eqn 16**). A tailing of the τ_i^{-1} distribution (i.e. Gaussian or exponential) towards higher frequencies is expected to produce a sub-linear

dependence of the integrated $G(\omega)$ vs ω, rather than a plateau. However, since the band bending is different from patch to patch, a patch-dependent D_S (determined by the position of the Fermi level at the interface) may also influence the shape of $G(\omega)$.

3. Experimental

Experimental methods including photochemical grafting, X-ray photoelectron spectroscopy (XPS), spectroscopic ellipsometry (SE), dc and ac electrical transport, were described in detail previously.[15] Covalent grafting of 1-dodecene ($C_{11}H_{22}$=CH_2) molecules (puriss, > 99%, Fluka) was performed on fully hydrogenated Si(111):H surfaces using a UV-assisted (λ = 300 nm) liquid phase process. In this study, no SiO_2 component could be observed near 103 eV on Si2p photoelectron spectra taken at α = 45° immediately after grafting of the dodecyl molecular layer. The optical thickness d_{SE} = 1.45 nm and the molecular coverage Σ_{ML} = 2.3×10^{14} cm^{-2} both indicate grafting of a rather dense C_{12} monolayer.

A low-doped *n*-type Si (1-10 Ω.cm, Siltronix) has been chosen to obtain rectifying junctions.[1,3,43-45] The doping density (N_D = 1.5×10^{14} cm^{-3}, as deduced from a Mott-Schottky plot of the high frequency capacitance, **Fig. 6b**) provides the position of the bulk Fermi level, $(E_C - E_{FB}) = qV_N = kT\ Ln(N_C / N_D)$ = 0.306 eV at 293 K, where N_C(cm^{-3}) = 2.8×10^{19} $(T / 300)^{1/2}$ is the effective density of states in the Si conduction band.

For current density $J(V, T)$ and admittance $Y(V, T, \omega)$ measurements, a home-made parallel plate sample holder has been designed to insert a mercury drop on top of the molecular junction.[15] This Teflon cell is inert towards mercury. A fresh mercury (99.999 % Fluka) drop (contact area S = 5×10^{-3} cm^2) was used to avoid electrical shorts through pinholes in the OML. An ohmic back contact was made by applying a silver paste electrode on the scratched Si backside (inset of **Fig. 4**). Dc and ac transport measurements were performed in a cryostat under

dry nitrogen flow to avoid water condensation and to minimize surface oxidation during the measurements.

J(*V*) characteristics were measured in the dark, using a Keithley 6487 picoammeter. Admittance measurements were carried out with a frequency response analyzer (Alpha-A High Resolution measurement system, Novocontrol Technologies) using a two terminal active cell.. Experiments with V_{AC} = 10 mV were carried out in two runs, a voltage sweep (waiting time 0.3 second / step 25 mV) and a frequency sweep (1×10^{-2} Hz to 1×10^{7} Hz), to study the measured complex admittance, $Y(V, T, \omega) = G_m + j\omega C_m$, against voltage, *V*, and frequency, $\omega/2\pi$.

The capacitance (4.5 pF) of the empty Teflon cell in parallel with the molecular junction was subtracted to obtain C_m. Here, high frequency and high forward bias admittance data were <u>not</u> corrected for the series resistance R_S (due to bulk Si and back contact resistance). R_S effects were rather included in the modelling using the high frequency value of the real part of the impedance, $R_S = G_m / (G_m^2 + \omega^2 C_m^2)$.[22] The R_S effect does not affect the excess capacitance $\hat{C}(0) - \hat{C}(\infty)$ or flat band voltage analysis; however, it broadens $M''(\omega)$ peaks and decreases the apparent response time.

4. Data analysis

A first criterion of the Hg // $C_{12}H_{25}$ – *n*-Si junction quality is given by a cyclic *C*(*V*) scan from 0 V to -4 V (depletion) to +0.8 V (accumulation near flat band conditions) to 0 V, performed immediately after grafting, which does not show detectable hysteresis at any frequency (from 10^2 Hz to 10^6 Hz) **(Figure 6a)**.

4.1 Current density

Direct current characteristics *J*(*V, T*) of the Hg // $C_{12}H_{25}$ – *n*-Si junction show a strong rectification which increases with decreasing temperature (**Fig. 4**). At low forward bias ($0 < V <$

0.4 Volt), the exponential $J(V)$ dependence, observed for all temperatures, is described by a thermionic emission (TE) mechanism. At high forward bias (V > +0.6 V), saturation in $J(V)$ and weak temperature dependence of $J(T)$ indicate that the current becomes limited by the tunnel barrier (TB) and by the contact resistance, rather than by the TE barrier inside the semiconductor. This behavior is typical of rectifying MIS tunnel junctions obtained previously with Hg // OML – *n* type Si.[1,3,43-45] In order to relate the applied voltage and the band bending, a full modeling of the current density, $J(V, T)$, characteristics has been reported elsewhere,[15] including the applied voltage partition between the tunnel barrier, the space charge in the semiconductor and the voltage drop on the series resistance. Note that the tunnel barrier model **(Eqn 3-5)** incorporates the dc charge carrier transport mechanisms (tunneling, thermionic emission) which were analyzed previously.[15]

4.2 Admittance characteristics

The frequency dependence of the admittance $Y(\omega)$ characteristics of the Hg // $C_{12}H_{25}$ – *n*-Si junction is shown in **Figures 5-7**. In **Figure 5**, the zero bias conductance $G(\omega)$ shows three frequency regimes in the range 1×10^{-2} Hz to 1×10^{7} Hz. Considering $G(\omega)$ at 243 K, at low frequencies (typically below 1 Hz), the conductance value $G(\omega \approx 0)$ is similar to the differential conductance $G = dJ/dV$ derived from the dc $J(V)$ characteristics in **Fig. 4**; from reverse to forward bias, it increases with increasing forward bias over seven decades (10^{-11} to 10^{-4} S.cm^{-2} at 243 K, not shown). At intermediate frequencies (typically above 1 Hz for reverse applied bias), a power law dependence, $G(\omega) \approx \omega^{p}$, is observed; it holds with an exponent p = 0.91±0.03 over nearly three decades in G (T = 243 K, V = 0 V). At high frequencies (typically above 1 MHz), the observed behaviour is dominated by the series resistance R_S which gives a quadratic frequency dependence of the measured conductance $G_m(\omega)$ as $\omega^2 C^2 R_S$; such behaviour is expected from a R//C circuit in series with a resistor R_S :

$$G_m(\omega) = \frac{G(1+GR_S)+\omega^2C^2R_S}{(1+GR_S)^2+\omega^2C^2R_S{}^2} \qquad (18)$$

if $(\omega_S\omega_{RC})^{1/2} \ll \omega \ll \omega_S$ where $\omega_S = (C\,R_S)^{-1}$ and $\omega_{RC} = (G/C)$.

As shown in **Figure 6**, the capacitance at reverse bias (V < +0.2 V) is low, C_{REV} = 10-20 pF (2-4 nF.cm^{-2}), at all frequencies, showing the formation of a depletion layer in the SC. It has been suggested that an inversion layer does not form because the hole tunnelling time is expected to be shorter than the generation-recombination time.[46] In weak depletion (+0.2 V < V < +0.7 V), $C(V)$ data reveal a strong frequency dependence which indicates the additional contribution of interface states at lower frequencies; in the equivalent circuit (inset **Fig. 6a**), they correspond to a parallel (R_{IT} // C_{IT}) component. The measured low frequency capacitance at high forward bias is larger than the geometric capacitance of the molecular insulator, C_i = 1.8 μF.cm^{-2}, expected from d_T = 1.5 nm and ε_i = 3.[3] This result, $C(0) > C_i$, is specific of ultrathin MIS tunnel junctions with a low tunnel barrier resistance R_T (equivalent circuit, inset **Fig. 6a**); this relation is predicted by **Eqn 14** if $q\beta J > C_i{}^2/(q^2D_S\tau)$, while the alternative condition, $D_S > C_i/q^2$ (corresponding to 1×10^{13} eV^{-1}.cm^{-2}), is very unlikely for a device-quality junction.

In order to validate **Equations 14-15** derived from the tunnel barrier model, **Figure 7** shows the "excess capacitance" defined as (C_{LF} - C_{HF}) = C(100 Hz) - C(1 MHz). The low frequency response has been arbitrarily taken at 100 Hz but a lower frequency could be chosen; on this junction, the 10 Hz capacitance is basically similar to the 100 Hz data at 293 K; however it shows a poorer signal / noise ratio (not shown). Note that this C(100 Hz) vs J behaviour is weakly dependent on the measurement temperature T in the range 253-293 K, except for the low currents dominated by the thermionic emission mechanism (**Figure 4**).

(i) For reverse and small forward bias (V < +0.25 V, J < 7×10^{-6} A.cm^{-2}) corresponding to a Fermi level position below mid-gap, C(100 Hz) is very similar to the high frequency capacitance C(1

MHz) (dashed line, C_{SC}, in **Figure 7**), because interface states below mid-gap are unable to respond to the ac voltage. Subtraction of the high frequency capacitance *C*(1 MHz) from *C*(100 Hz) leaves a very small low frequency contribution (0.4 nF.cm^{-2}) independent of *J* and *T* (for $J < 2\times10^{-7}$ A.cm^{-2}) ; in the depletion regime, this low frequency response adds to the semiconductor capacitance and thus explains the frequency shift in Mott-Schottky plots observed in **Fig. 6b**.

(ii) For larger forward bias (+0.25 V < *V* < +0.50 V, $J < 10^{-3}$ A.cm^{-2}) corresponding to a Fermi level position above mid-gap, a monotonic increase of the interface states response is essentially measured at $\omega \approx 100$ Hz ; in this regime, the capacitance of the depletion layer *C*(1 MHz) increases and remains smaller than *C*(100 Hz).

(iii) An abrupt transition occurs at *V* = +0.50 V ($J = 10^{-3}$ A.cm^{-2}) with a steep increase in the slope; this inflexion point (blue arrow in **Figure 7**) marks the onset of the "high current density regime", where $\hat{C}(0) - \hat{C}(\infty) \approx q^2 D_S(1 + q\beta J\tau/C_i)$ becomes dominated by the product $J D_S\tau$. At the transition, $q\beta J\tau \approx C_i$ provides the magnitude of the microscopic response time of interface defects, $\tau \approx 10$ µs.

(iv) Above this transition, in the very high current density regime ($J > 10^{-3}$ A.cm^{-2}) obtained for large forward bias (+0.5 V < *V* < +0.80 V), the dependence of the low frequency capacitance $C(\omega \approx 0)$ vs *J* is *superlinear*, because both *J* and D_S increase simultaneously. Interestingly, a linear dependence of *C*(100 Hz) as a function of the current density is recovered in the very high current density regime, typically above *J* = 15 mA.cm^{-2}, close to the flat band voltage, V_{FB} = 0.68 V (**Fig. 6b**). The inset in **Figure 7** (293 K) shows a linear dependence of $C(\omega \approx 0)$ vs *J* as expected from **Eqn 15** if D_S is weakly dependent on the applied forward bias; this condition can be met if the Fermi level is pinned in a high density of interface states located near the Si conduction band. This hypothesis is reasonable if one considers the magnitude of $D_S \approx 4\times10^{12}$ eV^{-1}.cm^{-2} derived from the experimental slope $(q^3 D_S\beta\tau/C_i)$ and the microscopic response time of interface defects, $\tau \approx 10$ µs.

4.3 Density of states distribution

To obtain a reliable distribution of the interface defect density, $D_S(E)$, close to the conduction band, we investigate the forward bias range where the admittance of the thin MIS diode is modified by a high current density. In the following, $D_S(E)$ is derived using three complementary methods: (i) the low-high frequency capacitance (or excess capacitance) method, strictly valid for thick MIS diodes,[22] (ii) the f^{LF} (or response time) method; (iii) the M_{MAX}^{LF} (or electrical modulus amplitude) method.

In the low-high frequency capacitance method, assuming J = 0, the ac response of interface traps due to the modulation of their average occupation is described by a parallel capacitance – resistance circuit in parallel with the space charge layer capacitance (inset of **Fig. 6a**). As shown in **Fig. 6a**, interface states do not respond at high frequencies, where the measured capacitance is essentially due to the SC; hence $D_S(E_C - E_T)$ can be obtained by subtracting the high frequency capacitance, $D_S = (C_{LF} - C_{HF})/qS$; this approximation holds because C_i is very large.

For the latter two methods, at each bias voltage, we use the measured electrical modulus (**Fig. 8a**) and the modulus calculated using the tunnel barrier model. The insulator capacitance is taken as C_i = 1.8 μF.cm^{-2}. An assumption has to be made on V_C and τ values **(Eqn. 7)**; using previous simulations,[35] V_C was taken at the bias giving an ideality factor equal to 1.15 (here qV_C = -3 kT) and the microscopic response time of interface defects, $\tau \approx 10$ μs, was obtained at the transition (blue arrow in **Figure 7**).

In the f^{LF} method (response time method reported previously[15]), admittance simulations use experimental $J(V)$ data (**Fig. 4**) and high frequency capacitance (1 MHz). D_S values are obtained by matching the calculated device response time $\tau_R(V, T, D_S)$ values with experimental values of the device response time (open dots in **Fig. 8b**) given by the frequency f^{LF} corresponding to the

maximum in the imaginary part of the modulus (M'') in **Fig. 8a**. In the electrical modulus amplitude method, we use the fact that M_{MAX}^{LF} decreases with increasing D_S (**Fig. 3b**). Note that the current density was assumed to remain constant ($J = 1\times10^{-7}$ A.cm^{-2}) in this set of simulations. The corresponding values have been reported in **Fig. 8c** (blue dots).

The role of a high J through the MIS tunnel diode can be assessed by comparing the energy distributions of interface defects resulting from the different methods. The results shown in **Fig. 8c** globally confirm the low D_S values ($D_S < 10^{11}$ eV^{-1}.cm^{-2}) near mid-gap for the $C_{12}H_{25}$ – *n* Si interface. They indicate that the exponential increase in $D_S(E_C - E_T)$ near the conduction band derived from the low-high frequency capacitance method is overestimated due to the large dc current density; however, the low-high frequency capacitance method appears to be reliable up to 1 mA.cm^{-2} (here $V \leq 0.45$ V). In contrast, the M_{MAX}^{LF} method (within the low J approximation) underestimates $D_S(E)$ as compared with the response time method.

5. Discussion

Before discussing the effect of the high current density, let us recall that several mechanisms may also affect the dynamic response of the MIS tunnel device, namely lateral inhomogeneity and dipolar relaxation effects.[42]

The power law dependence of the measured conductance, $G(\omega)$, is very different from the high frequency plateau expected for a MIS tunnel device with homogeneous barrier height. Similarly, some unexpected plateau appears over a broad frequency range in $M''(\omega)$ plots (**Fig. 8a**, reverse bias). As discussed in **Section 2.4**, this indicates that the junction has a distribution of low barrier height patches or thinner tunnel barriers. This conclusion is consistent with low temperature dc current characteristics of molecular tunnel junctions.[42] Note that the excess capacitance will be less affected than the excess conductance since the space charge layer

thickness is weakly dependent on the interface potential fluctuations. Hence, we expect that the homogeneous model still applies to experimental excess capacitance results.

For reverse and small forward bias (V < +0.25 V, J < 7×10^{-6} A.cm^{-2}) corresponding to a Fermi level position below midgap, interface states are unable to respond to the ac voltage. The observed very small low frequency capacitance being independent on temperature (in the investigated range 243-293 K), it is rather attributed to some dipolar relaxation in the molecular monolayer, likely due to interface Si-C bond dipoles, in the absence of any detectable silicon oxide SiO_x component in XPS spectra (Si2p core level, $\alpha = 45°$, not shown). This low frequency contribution (0.5 nF.cm^{-2}), attributed to Si-C interface dipoles of the fresh Hg // $C_{12}H_{25}$ – Si device, is much smaller than the dipolar capacitance values (30-40 nF.cm^{-2}) reported in a recent admittance study of alkyl (C_{18} – n^+ Si) molecular assemblies.[14]

In MIS tunnel junctions with molecular insulator, low dipolar contribution is an important condition to detect a small surface states response, since the latter may be masked by any dipolar relaxation of interface or embedded polar moieties. As an illustration, in a study of long term stability of molecular devices (ageing at the ambient for eighteen months), a significant increase has been observed in the dipolar relaxation capacitance (x 50) and in the interface states response (x 7) of the Hg // $C_{12}H_{25}$ – Si junction; besides the appearance of an interface silicon oxide layer revealed by XPS, some presence of adsorbed water vapour cannot be excluded.[42] This effect could be possibly delayed or suppressed by engineering a very compact molecular layer.[47]

To understand the admittance response of interface states, we have proposed a representation of the excess capacitance, (C_{LF} - C_{HF}), as a function of the dc current density, J, which clearly reveals the different regimes predicted by modelling the non equilibrium tunnel MIS junction in the forward bias range. Interestingly, the admittance behavior can be mapped onto the dc transport mechanisms[15]: (i) in the *low current density* regime, the response of interface states above midgap is unaffected, corresponding to a current density limited by thermionic emission

over the barrier in silicon; (ii) in the *high current density* regime (J > 1 mA.cm^{-2}), the admittance depends strongly on both the density of localized states and the dc current density, corresponding to a current density limited by tunneling through the molecular barrier.

At low current density values, a good agreement is found between the interface states distributions $D_S(E)$ derived from modeling of the device response frequency f^{LF} and modulus amplitude M_{MAX}^{LF} values, as compared with the low–high frequency capacitance method valid for thick MIS devices. Hence, for the $C_{12}H_{25}$ – *n* Si interface, the latter method appears to be reliable up to 1 mA.cm^{-2}. Future work is required to understand the discrepancies between f^{LF} and M_{MAX}^{LF} methods, which appear at intermediate current densities (**Figure 8c**).

The microscopic tunnel response time ($\tau = 10$ µs for the $C_{12}H_{25}$ – *n* Si interface) has been derived from the inflexion point in the excess capacitance, which marks the onset of the high current density regime (**Eqn 15)**. This derivation requires an accurate estimate of the insulator capacitance per unit area; however, in ultra thin MIS diodes, C_i cannot be obtained from the measured capacitance saturation at high forward bias, in contrast with thick MIS.

In **Figure 7**, some increase in the $C(\omega \approx 0)$ values at high current density has been observed after the first voltage scan (up to 0.8 V) at 293 K. Subsequent scans at lower temperatures (273 K and 253 K) show reproducible $C(\omega \approx 0)$ vs J plots. Hence, more work is needed to understand the detailed shape of the $C(\omega \approx 0)$ - $C(\omega \approx 1$ MHz) vs J plots at very high current densities, e.g. by performing ageing studies at the ambient or under high bias-stress conditions. In particular, it will be interesting to check if the linear part of the $C(\omega \approx 0)$ vs J plot is observed in all molecular MIS diodes or if it is rather an accidental effect.

6. Conclusion

Modifications of the measured admittance induced by a high current density in ultrathin MIS devices have been investigated in order to obtain reliable values of the density distribution, $D_S(E)$, of defects localized at the semiconductor interface. The behavior of admittance and current density characteristics has been illustrated using Hg // $C_{12}H_{25}$ – Si junctions incorporating 1-2 nm thick alkyl molecular layers covalently bonded to Si(111); using *n*-type silicon, the rectifying characteristics provide a very wide range of current densities.

Modeling the forward bias admittance of non equilibrium tunnel junctions reveals several regimes which can be observed either in $C(\omega \approx 0)$ vs (J) plots of the low frequency capacitance over six decades in current or in $M''(\omega)$ plots of the electrical modulus over eight decades in frequency. At low current density, the response of interface states above mid-gap is unaffected and a good agreement is found between the interface states densities derived from the modeling of either device response time $\tau_R(V)$ and magnitude of the electrical modulus $M''(\omega)$, as compared with the low–high frequency capacitance method valid for thick MIS devices; the low value of $D_S(E)$ near mid-gap (D_S < 1×10^{11} $eV^{-1}.cm^{-2}$) indicates good passivation of dangling bonds at the $C_{12}H_{25}$ – *n* Si interface.

In the high current density regime (J > 1 $mA.cm^{-2}$), the admittance depends strongly on both the density of localized states and the dc current density, so that the excess capacitance method overestimates D_S. For very high current densities (J > 10 $mA.cm^{-2}$), the linear $C(\omega \approx 0)$ vs (J) dependence could indicate some Fermi level pinning in a high interface density of states near the Si conduction band.

The $C(\omega \approx 0)$ vs (J) representation of dynamic characteristics of molecular layers covalently immobilized on Si(111) is also interesting to discriminate dipolar relaxation effects from interface states response. The temperature-independent excess capacitance $C(\omega \approx 0)$ - C(1 MHz) observed

at very small current density, not predicted by the admittance model, is attributed to some dipolar relaxation in the molecular junction. Dipolar relaxation effects may obscure the interface states response for molecular insulator with strong interface or embedded dipolar moieties.

Acknowledgments

We wish to thank Jean-Paul Kleider (CNRS) for fruitful suggestions about transport mechanisms, Bruno Fabre and Cyril Herrier (CNRS - University of Rennes 1) for molecular grafting, Roopa Hiremath for some admittance measurements, Cristelle Mériadec for some XPS characterizations, Région Bretagne and Rennes Métropole for their financial support.

REFERENCES

[1] Salomon A, Boecking T, Seitz O, Markus T, Amy F, Chan CK, et al. What is the Barrier for Tunneling Through Alkyl Monolayers? Results from *n*- and *p*-Si–Alkyl/Hg Junctions. Adv Mater 2007;19:445-50.

[2] Har-Lavan R, Ron I, Thieblemont F, Cahen D. Toward metal-organic insulator-semiconductor solar cells, based on molecular monolayer self-assembly on *n*-Si. Appl Phys Lett 2009;94:043308.

[3] Faber EJ, de Smet LCPM, Olthuis W, Zuilhof H, Sudholter EJR, Bergveld P, et al. Si-C Linked Organic Monolayers on Crystalline Silicon Surfaces as Alternative Gate insulators. ChemPhysChem 2005;6:2153-66.

[4] Aswal DK, Lenfant S, Guerin D, Yakhimi JV, Vuillaume D. Self assembled monolayers on silicon for molecular electronics. Anal Chimica Acta 2006;568:84-108.

[5] Lindsay SM, Ratner MA. Molecular Transport Junctions: Clearing Mists. Adv Mater 2007;19:23-31.

[6] Vuillaume D. New concepts for nanophotonics and nano-electronics. Molecular-scale electronics. CR Physique 2008;9:78-94.

[7] Vilan A, Yaffe O, Biller A, Salomon A, Kahn A, Cahen D. Molecules on Si: Electronics with chemistry. Adv Mater 2010;22:140-59.

[8] Ghosh AW, Electronics with molecules, *Comprehensive Semiconductor Science and Technology* (Elsevier, Amsterdam, 2011), Chap. 5.09, pp. 383-479.

[9] Linford MR, Chidsey CED. Alkyl monolayers covalently bonded to silicon surfaces. J Am Chem Soc 1993;115:12631-2.

[10] Royea WJ, Juang A, Lewis NS. Preparation of air stable, low recombination velocity Si(111) surfaces through alkyl termination. Appl Phys Lett 2000;77:1988-90.

[11] Lehner A, Kohl F, Franzke SA, Graf T, Brandt MS, Stutzmann M. Photoconductivity and spin dependent photoconductivity of hydrosylilated (111) silicon surfaces. Appl Phys Lett 2003;82:565-7.

[12] Kar S, Miramond C, Vuillaume D. Properties of electronic traps at silicon/1-octadecene interfaces. Appl Phys Lett 2001;78:1288-90.

[13] Kar S. Study of silicon-organic interfaces by admittance spectroscopy. Appl Surf Sci 2006;252:3961-7.

[14] Clement N, Pleutin S, Guerin D, Vuillaume D. Relaxation dynamics in covalently bonded organic monolayers on silicon. Phys Rev B 2010;82:035404.

[15] Fadjie-Djomkam AB, Ababou-Girard S, Hiremath R, Herrier C, Fabre B, Solal F, Godet C. Temperature dependence of current density and admittance in metal-insulator-semiconductor junctions with molecular insulator. J Appl Phys 2011;110:083708.

[16] Thuo MM, Reus WF, Nijhuis CA, Barber JR, Kim C, Schulz MD, Whitesides GM. Odd-even effects in charge transport across self-assembled monolayers. J Am Chem Soc 2011;133:2962-75.

[17] Smaali K, Clement N, Patriarche G, Vuillaume D. Conductance statistics from a large array of sub-10 nm molecular junctions. ACS Nano 2012;6: 4639–4647.

[18] Sze SM. *Semiconductor devices: Physics and Technology*, Wiley, New York, 1985.

[19] Card HC, Rhoderick EH. Studies of tunnel MOS diodes I. Interface effects in silicon Schottky diodes. J Phys D: Appl Phys 1971;4:1589-601.

[20] Wu CY. Interfacial layer theory of the Schottky barrier diodes. J Appl Phys 1980;51:3786-89.

[21] Wu CY. Interfacial layer-thermionic-diffusion theory for the Schottky barrier diode. J Appl Phys 1982;53:5947-50.

[22] Nicollian EH, Brews JR. *MOS (Metal Oxide Semiconductor) Physics and Technology*, Wiley, New York, 1982.

[23] Castagne R, Vapaille A. Description of the SiO_2-Si interface properties by means of very low frequency MOS capacitance measurements. Surf Sci 1971;28:157-193.

[24] Tseng HH, Wu CY. A simple interfacial model for the non-ideal I-V and C-V characteristics of the Schottky-barrier diode. Solid-State Electron 1987;30:383-90.

[25] Werner J, Ploog K, Queisser HJ. Interface states measurements at Schottky contacts: a new admittance technique. Phys Rev Lett 1986;57:1080-4.

[26] Kar S, Dahlke WE. Interface states in MOS structures with 20-40 Å thick SiO_2 films on nondegenerate Si. Solid-State Electron 1972;15:221-37.

[27] Viktorovitch P. Bulk and surface states analysis in a-Si:H by Schottky and MIS tunnel diodes capacitance and conductance measurements. J Appl Phys 1981;52:1392-404.

[28] Ouennoughi Z, Sella A. MIS tunnel admittance with an inhomogeneous dielectric. Int J Electron 1997;83:571-80.

[29] Chattopadhyay P. Admittance of metal-insulator-semiconductor tunnel contacts in the presence of donor-acceptor mixed interface states and interface reaction. J Appl Phys 2001;89:364-373.

[30] Liu YJ, Yu HZ. Molecular passivation of mercury-silicon (p-type) diode junctions: alkylation, oxidation, and alkylsilation. J Phys Chem B 2003;107:7803-11.

[31] Pleutin S, Clement N, Guerin D, Vuillaume D. Molecular relaxation dynamics in organic monolayer junctions. Phys Rev B 2010;82:125436.

[32] Scott MC, Stevens DR, Bochinski JR, Clarke LI. Dynamics within alkylsiloxane self-assembled monolayers studied by sensitive dielectric spectroscopy. ACS Nano 2008;2: 2392–2400.

[33] Zhang Q, Zhang Q, Archer LA. Molecular relaxation dynamics of self-assembled monolayers. J Phys Chem B 2006;110:4924.

[34] Sune J, Oriols X, Autran JL. Non-equilibrium gate tunneling current in ultra-thin (<2 nm) oxide MOS devices. J Non-Cryst Solids 2001;280:127-131.

[35] Gomila G, Rubi JM. Relation for the nonequilibrium population of the interface states: Effects on the bias dependence of the ideality factor. J Appl Phys 1997;81:2674-81.

[36] Gomila G. Effects of interface states on the non-stationary transport properties of Schottky contacts and metal-insulator-semiconductor tunnel diodes. J Phys D: Appl Phys 1999;32:64-71.

[37] Werner JH. Electrical characterization of interface states at Schottky contacts and MIS tunnel diodes. In *Metallization and Metal-semiconductor interface states* (Plenum, New York, 1989), pp. 235-56.

[38] Chattopadhyay P, Raychaudhury B. Frequency dependence of forward capacitance-voltage characteristics of Schottky barrier diodes. Solid-State Electron 1993;36:605-610.

[39] Werner JH, Güttler HH. Barrier inhomogeneities at Schottky contacts. J Appl Phys 1991;69:1522-1533.

[40] Sullivan JP, Tung RT, Pinto MR, Graham WR. Electron transport of inhomogeneous Schottky barriers : A numerical study. J Appl Phys 1991;70:7403-7424.

[41] Tung RT. Recent advances in Schottky barrier concepts. Mat Sci Eng R 2001;35:1-138.

[42] Fadjie-Djomkam AB, Ababou-Girard S, Godet C. Barrier height distribution and dipolar relaxation in metal-insulator-semiconductor junctions with molecular insulator: ageing effects. J Appl Phys 2012. [http://dx.doi.org/10.1063/1.4767121]

[43] Salomon A, Boecking T, Chan CK, Amy F, Girshevitz O, Cahen D, Kahn A. How Do Electronic Carriers Cross Si-Bound Alkyl Monolayers? Phys Rev Lett 2005;95:266807.

[44] Maldonado S, Plass KE, Knapp D, Lewis NS. Electrical Properties of Junctions between Hg and Si(111) Surfaces Functionalized with Short-Chain Alkyls. J Phys Chem C 2007;111:17690–9.

[45] Godet C, Fadjie A, Ababou-Girard S, Solal F. Tunnel barrier parameters derivation from normalized differential conductance in Hg / organic monomolecular layer-Si junctions. Appl Phys Lett 2010;97:132105.

[46] Kar S. Determination of minority carrier lifetime using MIS tunnel diodes. Appl Phys Lett 1974;25:587-9.

[47] Clement N, Guerin D, Pleutin S, Godey S, Vuillaume D. Role of hydration on the electrical transport through molecular junctions on silicon. J Phys Chem C 2012;116:17753–63.

FIGURE CAPTIONS

Figure 1 Energy band diagram and carrier exchange mechanisms at the tunnel MIS interface[36] (reprinted with permission from IOP).

Figure 2 Simulation of capacitance $C(\omega)$, conductance $G(\omega)$ and imaginary electrical modulus $M''(\omega)$ of the MIS tunnel junction using measured $J(V)$ (**Fig. 4**, 293 K) and capacitance at 1 MHz. Continuous lines: at +0.2 V forward bias for variable density of interface states, D_S, in the range $10^{10} – 3\times10^{12}$ $eV^{-1}.cm^{-2}$. Symbols: at fixed $D_S = 3x10^{12}$ $eV^{-1}.cm^{-2}$ for variable forward bias.

Figure 3 a) Simulation of $M''(\omega)$ peaks (using $J = 1\times10^{-7}$ $A.cm^{-2}$, $C_i = 1.8$ $\mu F.cm^{-2}$, $C_{SC} = 3.6$ $nF.cm^{-2}$); b) dependence of characteristic frequencies, f^{LF} and f^{HF}, and magnitude of the modulus peak values, M_{MAX}^{LF} and M_{MAX}^{HF}, as a function of D_S.

Figure 4 Temperature dependence of current density $J(V)$ characteristics of a Hg // $C_{12}H_{25}$ – *n*-Si junction in the range 243-293 K (step 10 K). Inset: schematic of the MIS structure (note that the molecular layer thickness is not scaled) inserted within the Teflon cell.

Figure 5 Frequency dependence of the measured conductance of a Hg // $C_{12}H_{25}$ – *n*-Si junction at zero bias and variable temperature T (243 K to 293 K) ; in the intermediate frequency range, a power-law behaviour is observed ($p = 0.91$ at 253 K) with a trend towards saturation above 10^5 Hz sketched by the dotted line. The series resistance, R_S can be obtained from the high frequency regime where $G(\omega)$ is proportional to ω^2.

Figure 6 Frequency dependence of the measured capacitance of a Hg // $C_{12}H_{25}$ – *n*-Si junction at T = 253 K : a) $C_m(V)$ from 100 Hz to 1 MHz showing the absence of hysteresis, b) Mott-Schottky plot (C_m^{-2} vs V) giving the flat band voltage; the shift in the reverse bias range is attributed to a small dipolar relaxation component.

Figure 7 Excess capacitance (C_{LF} - C_{HF}) as a function of the dc current density in a Hg // $C_{12}H_{25}$ – *n*-Si junction at T = 293 K (red crosses), 273 K (blue dots) and 253 K (green triangles). The voltage scale and the inset correspond to 293 K data. The inflection point (vertical arrow) corresponds to the transition between the low (TE limited) and the high (tunnel limited) current density regimes. The horizontal baseline (2 pF or 0.4 nF.cm^{-2}) is attributed to a small dipolar relaxation component.

Figure 8 : a) Experimental $M''(\omega)$ of a Hg // $C_{12}H_{25}$ – *n*-Si junction measured at 293 K for increasing bias applied on Hg (-0.8 V, -0.5 V, -0.2 V, -0.05 V, 0 V, +0.05 V, +0.1 V, +0.2 V, +0.3 V, +0.4 V, +0.5 V, +0.6 V, +0.7 V, +0.8 V); b) experimental response time (circles) compared with simulated values (lines) using variable density of interface states D_S from 1×10^{10} to 3×10^{12} eV^{-1}.cm^{-2} (measured $J(V)$ were used as input in the simulation) ; c) energy dependence of the density of interface states $D_S(E_C - E_T)$ derived from experimental data using the low-high frequency capacitance method (black triangles), the f^{LF} method (open squares), and the M_{MAX}^{LF} method (full circles) as described in Section 4.3. The Fermi level is at mid gap for a forward applied bias of +0.25 V.

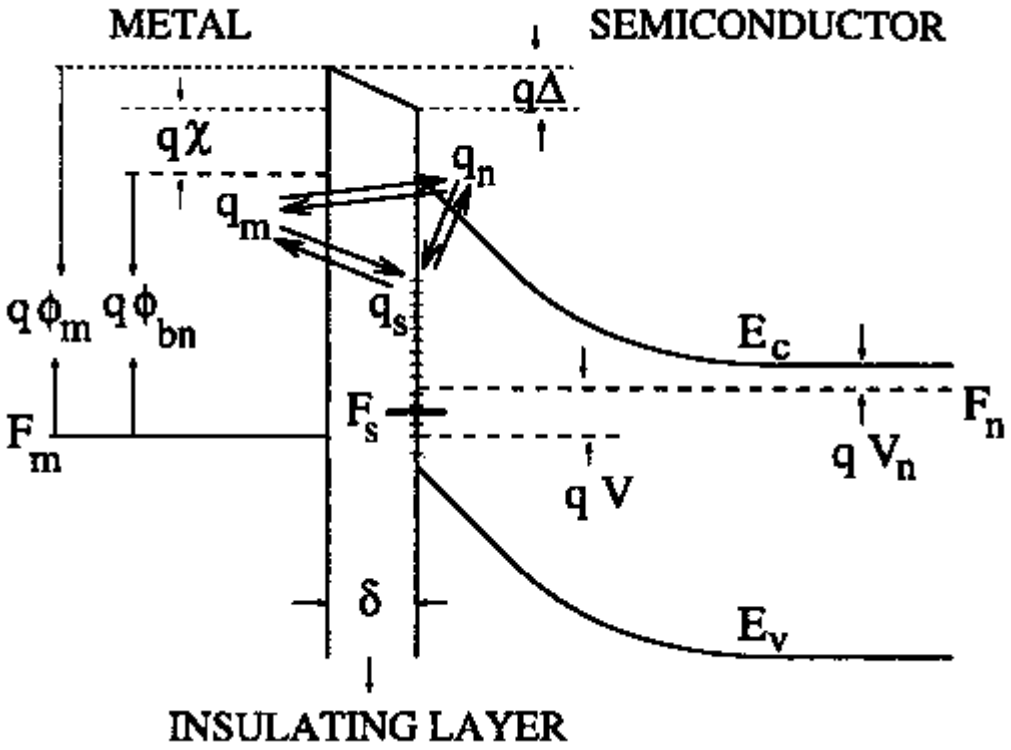
METAL
SEMICONDUCTOR
qΔ
qχ
q_n
q_m
$q\phi_m$
$q\phi_{bn}$
q_s
E_c
F_n
F_m
F_s
qV_n
qV
δ
E_v
INSULATING LAYER

Figure 1

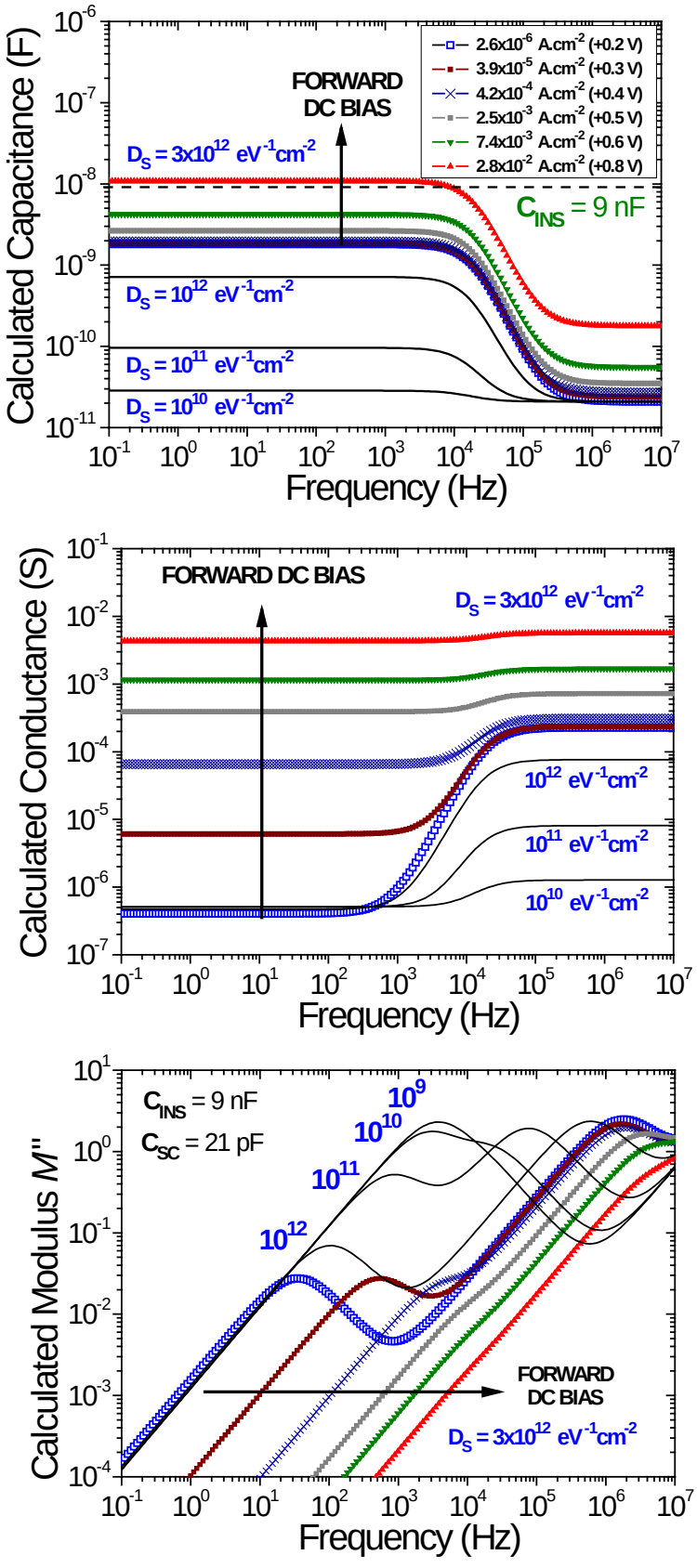
Calculated Capacitance (F)
Frequency (Hz)
FORWARD
DC BIAS
2.6x10-6 A.cm-2 (+0.2 V)
3.9x10-5 A.cm-2 (+0.3 V)
4.2x10-4 A.cm-2 (+0.4 V)
2.5x10-3 A.cm-2 (+0.5 V)
7.4x10-3 A.cm-2 (+0.6 V)
2.8x10-2 A.cm-2 (+0.8 V)
DS = 3x10^12 eV-1cm-2
CINS = 9 nF
DS = 10^12 eV-1cm-2
DS = 10^11 eV-1cm-2
DS = 10^10 eV-1cm-2
Calculated Conductance (S)
FORWARD DC BIAS
DS = 3x10^12 eV-1cm-2
10^12 eV-1cm-2
10^11 eV-1cm-2
10^10 eV-1cm-2
Calculated Modulus M''
CINS = 9 nF
CSC = 21 pF
10^9
10^10
10^11
10^12
FORWARD
DC BIAS
DS = 3x10^12 eV-1cm-2

Figure 2

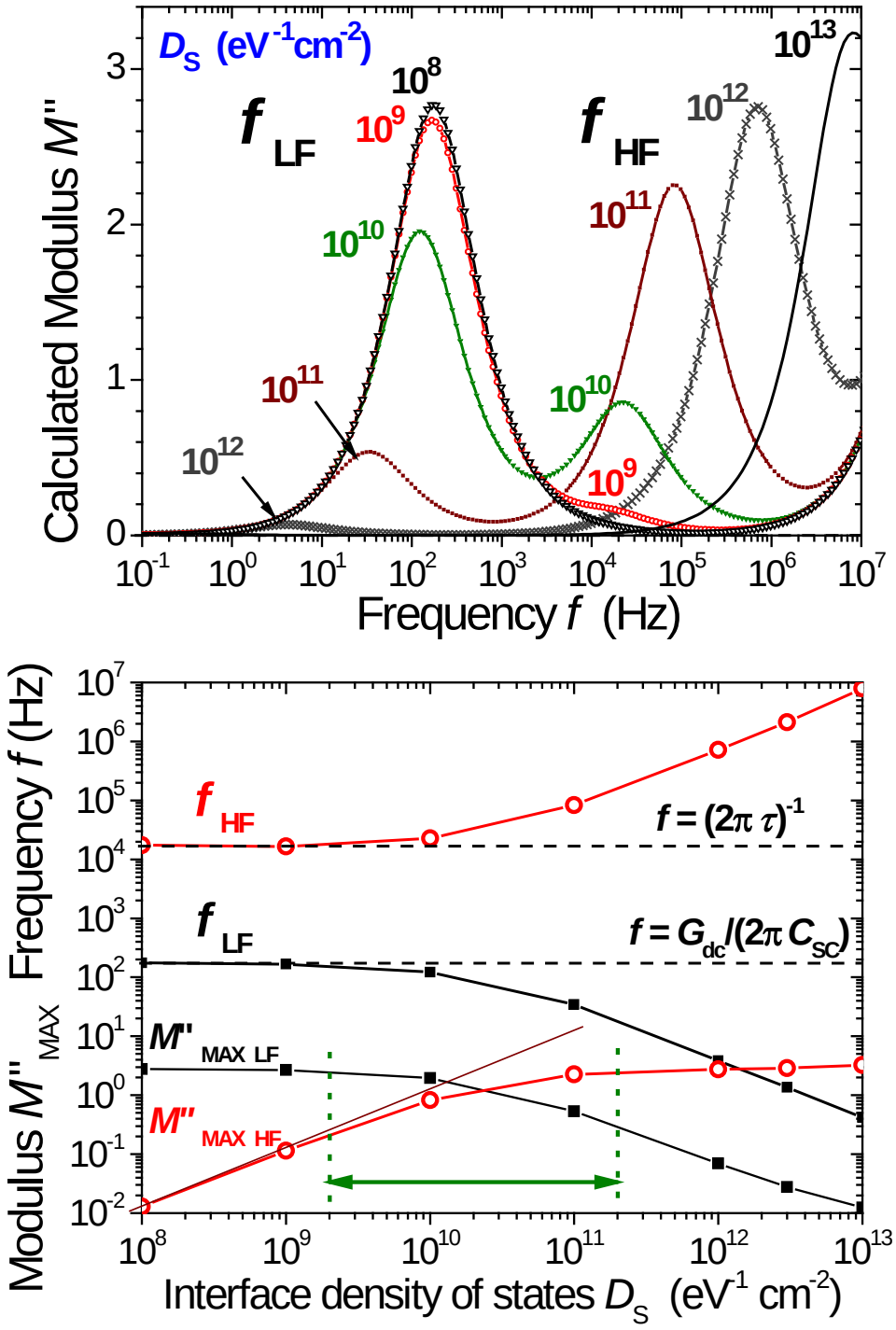
D_S (eV^{-1}cm^{-2})
10^8
10^9
10^{10}
10^{11}
10^{12}
10^{13}
f_{LF}
f_{HF}
Calculated Modulus M''
Frequency f (Hz)
Frequency f (Hz)
f_{HF}
$f = (2\pi\tau)^{-1}$
f_{LF}
$f = G_{dc}/(2\pi C_{SC})$
M'' MAX
M' MAX LF
M'' MAX HF
Interface density of states D_S (eV^{-1} cm^{-2})

Figure 3

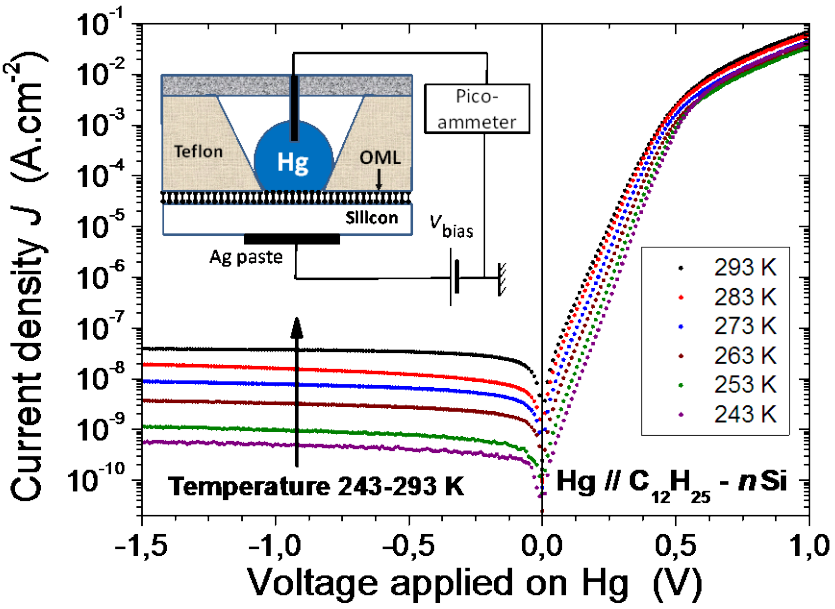
Current density J (A.cm-2)
Voltage applied on Hg (V)
Teflon
Hg
OML
Silicon
Ag paste
Pico-ammeter
Vbias
293 K
283 K
273 K
263 K
253 K
243 K
Temperature 243-293 K
Hg // C12H25 - nSi

Figure 4

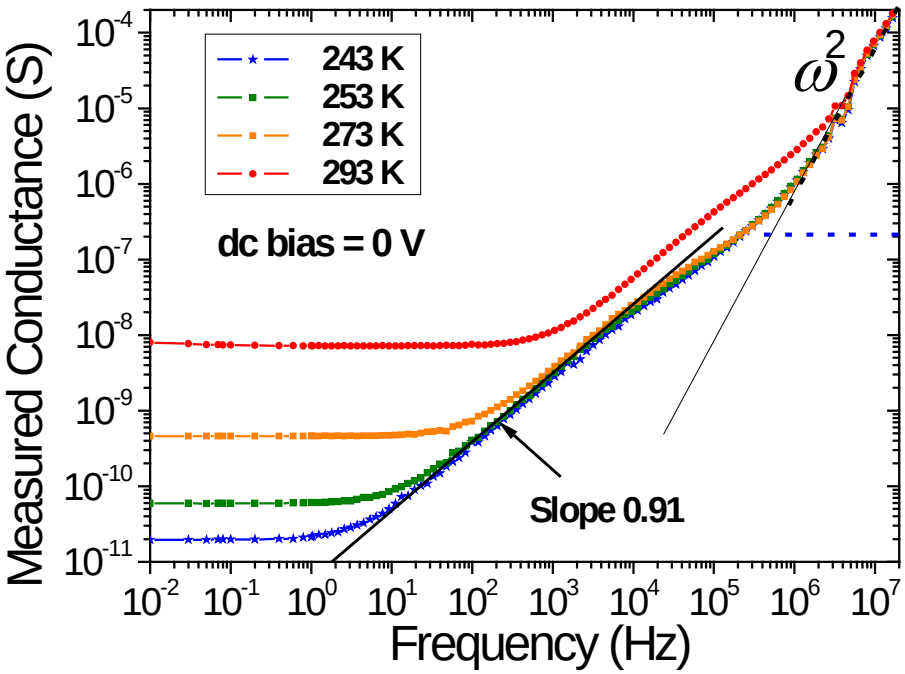
243 K
253 K
273 K
293 K
dc bias = 0 V
ω^2
Slope 0.91
Measured Conductance (S)
Frequency (Hz)
10^{-4}
10^{-5}
10^{-6}
10^{-7}
10^{-8}
10^{-9}
10^{-10}
10^{-11}
10^{-2} 10^{-1} 10^{0} 10^{1} 10^{2} 10^{3} 10^{4} 10^{5} 10^{6} 10^{7}

Figure 5

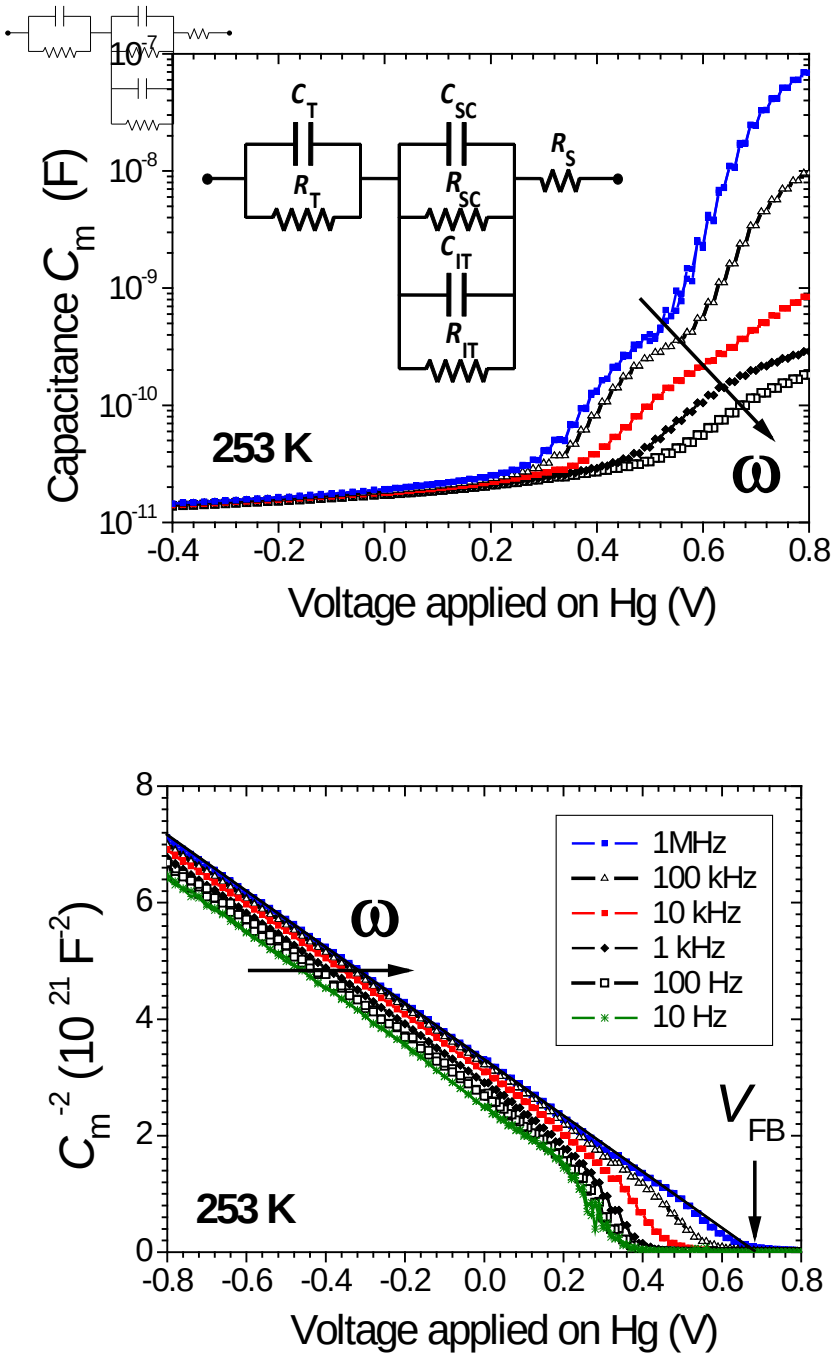
Capacitance C_m (F)
Voltage applied on Hg (V)
C_T
R_T
C_{SC}
R_{SC}
C_{IT}
R_{IT}
R_S
253 K
ω
C_m^{-2} (10^{21} F^{-2})
1MHz
100 kHz
10 kHz
1 kHz
100 Hz
10 Hz
V_{FB}

Figure 6

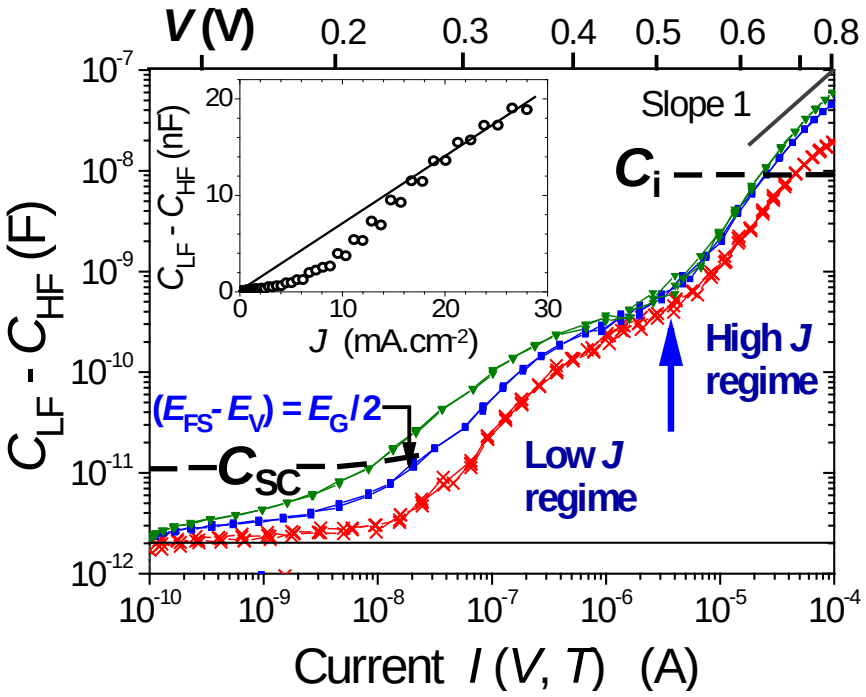
V (V)
0.2
0.3
0.4
0.5
0.6
0.8
Slope 1
C_i
C_{LF} - C_{HF} (F)
C_{LF} - C_{HF} (nF)
J (mA.cm^{-2})
High J regime
Low J regime
$(E_{FS}-E_V) = E_G/2$
C_{SC}
Current I (V, T) (A)

Figure 7

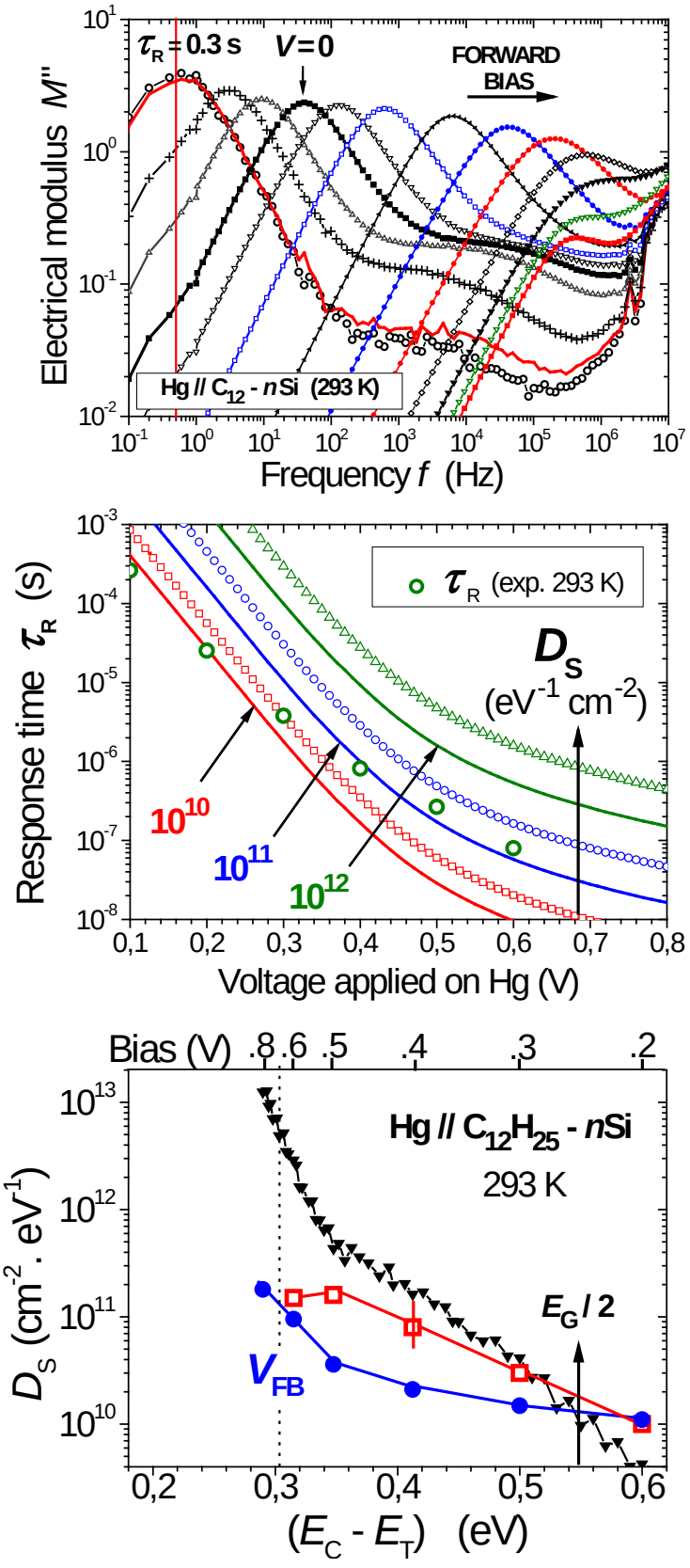
τR = 0.3 s
V = 0
FORWARD BIAS
Hg // C12 - nSi (293 K)
Electrical modulus M''
Frequency f (Hz)
τR (exp. 293 K)
DS (eV-1 cm-2)
10^10
10^11
10^12
Response time τR (s)
Voltage applied on Hg (V)
Bias (V)
Hg // C12H25 - nSi
293 K
EG / 2
VFB
DS (cm-2 . eV-1)
(EC - ET) (eV)

Figure 8